Prediction of near-field shear dispersion in an emergent canopy with heterogeneous morphology

Running head: Near-field shear dispersion in a canopy

Article Type: Short Communication

Title: Prediction of near-field shear dispersion in an emergent canopy with heterogeneous morphology

Authors: A. F. Lightbody and H. M. Nepf

Affiliation: Ralph M. Parsons Laboratory, Department of Civil and Environmental Engineering, Massachusetts Institute of Technology

Address for correspondence:

Anne Lightbody

Ralph M. Parsons Laboratory

Department of Civil and Environmental Engineering

Massachusetts Institute of Technology

77 Massachusetts Avenue, 48-216

Cambridge, MA 02139 USA

Tel: (617) 899-8449

Fax: (617) 253-7475

lightbod@mit.edu

Abstract

The evaluation of longitudinal dispersion in aquatic canopies is necessary to predict the behavior of dissolved species and suspended particles in marsh and wetland systems. Here we consider the influence of canopy morphology on longitudinal dispersion, focusing on transport before constituents have mixed over depth. Velocity and longitudinal dispersion were measured in a model canopy with vertically varying canopy density. The vertical variation in canopy morphology generates vertical variation in the mean velocity profile, which in turn creates mean-shear dispersion. We develop and verify a model that predicts the mean-shear dispersion in the near field from morphological characteristics of the canopy, such as stem diameter and frontal area. Close to the source, longitudinal dispersion is dominated by velocity heterogeneity at the scale of individual stems. However, within a distance of approximately 1 m, the shear dispersion associated with velocity heterogeneity over depth increases and eclipses this smaller-scale process.

Key words: Canopy, diffusion, dispersion, element array, near field, shear, vegetation, velocity

Abbreviations:

A – cross-sectional area

a – volumetric frontal area density

C_D – drag coefficient

d – stem diameter

D_z – vertical turbulent diffusion coefficient

f – function

g – gravitational constant

h – water depth

i – variable

K – dispersion coefficient

n – stem density

O – order of magnitude

Q – volumetric flow rate

Re_d – stem Reynolds number

t – time

u – local time-averaged fluid velocity

$\langle u \rangle$ – local time- and horizontally averaged fluid velocity

U – time- and depth-averaged fluid velocity

x – distance in the direction of flow

y – transverse coordinate

z – height above bed

β – scale constant

Δh – effective vertical cloud width

$\Delta \langle u \rangle$ – difference between maximum and minimum velocities

η – surface elevation

ν – kinematic viscosity

σ_x – concentration standard deviation

σ_x^2 – spatial concentration variance

1. Introduction

Advection and dispersion in obstructed flows play an important role in the ecology of many environmental systems. In groundwater flows, the interaction of flow with the grain matrix or lenses of varied porosity may result in the spread of a toxic contaminant plume, with acute effects on human health [1]. In wetland systems, many arthropods and macrophytes rely on water currents for the passive dispersal of larval stages and seeds [2, 3]. Furthermore, larger organisms rely on chemical signals in the water column for information necessary for foraging and mating, and these signals may be mediated by flow through the aquatic canopy [4].

Because vertical mixing is slow within wetland canopies, it is often important to understand dispersion processes before the constituent of interest has mixed across the full water depth, i.e., in the near field. For example, in a salt marsh canopy, the depth-averaged fluid velocity $U = O(1\text{–}5\ \text{cm/s})$, the vertical turbulent diffusion coefficient $D_z = O(0.1\ \text{cm}^2/\text{s})$, and the water depth $h = O(10\text{–}50\ \text{cm})$ [5, 6]. Under these conditions, a constituent will not mix over depth until a time scale of $t \sim h^2/D_z = O(1000\text{–}10,000\ \text{s})$, or a distance in the direction of flow of $x = O(10\text{–}1000\ \text{m})$. This paper explores models for characterizing the spread of a cloud at time- and length-scales less than these limits, which is a region of interest for many important processes, such as seed dispersal and chemical signaling.

2. Theoretical development

An emergent vegetative canopy can be characterized by the length scale of the stems, here assumed to be their diameter d; the stem density n; and the volumetric frontal area density $a = nd$. The solid volume fraction is approximately ad. In most wetland canopies, $ad < 0.1$ [5, 6] , although Mazda *et al.* [7] report that in mangrove canopies ad can be as high as 0.4. The time-averaged fluid velocity u varies at the scale of the stem in both the longitudinal (x) and transverse (y) directions due to wakes that form behind each stem. We define a horizontally averaged velocity within the fluid volume, $\langle u \rangle$. Following Ayotte *et al.* [8], this spatial average is taken over a length scale much greater than the individual stem spacing but less than the length scale of horizontal variation in frontal area density, a. The depth average of $\langle u \rangle$ is $U = Q/[A(1 - ad)]$, where Q is the volumetric flow rate and A the total cross-sectional area perpendicular to the flow.

When a varies with height above the bed z (see Fig. 1), there are two length scales of velocity variation within the canopy: variation at the scale of the stem due to fluctuations in $u(x, y)$ and variation due to the mean velocity shear $\langle u \rangle = f(z)$. Both of these velocity fluctuations contribute to dispersion. Further, when properly defined, these individual dispersive processes are additive. For $ad < 0.1$, the stem-scale dispersion, characterized by the coefficient K_d, is dominated by the wake-shear dispersion, which becomes Fickian after a distance $x > a^{-1}$ [9, 10]. After this point, for $ad < 0.1$, K_d can be represented by [9]:

$$K_d = \frac{1}{2}\langle u \rangle d\, C_D^{1.5} \tag{1}$$

where C_D is a non-dimensional drag coefficient. To simplify the expression given by White and Nepf [9], we have taken the recommended values for constants given in that paper.

To characterize the mean-shear dispersion, we must first characterize the velocity variation over depth. Under steady, uniform, two-dimensional flow through an emergent canopy, the longitudinal momentum equation reduces to a balance between the drag and pressure forces, i.e.,

$$\frac{1}{2} C_D a \langle u \rangle^2 = g \frac{\partial \eta}{\partial x} \tag{2}$$

where g is the gravitational constant and $\partial \eta / \partial x$ is the water surface slope. Strictly speaking the pressure term (right-hand side of Eq. 2) should account for the effect of porosity $(1 - ad)$, but we will neglect it here for a canopy with $ad < 0.1$. The drag coefficient C_D is a function of the stem Reynolds number Re_d = $\langle u \rangle d/\nu$, where ν is the kinematic viscosity of water. Empirical relations are well established for the drag coefficient on an isolated object between $1 < Re_d < 1000$ (e.g., [11]). The exact behavior of the drag coefficient within an array at a moderate Reynolds number is not as well understood, but, for an array of cylinders with $ad < 0.1$ and $Re_d > 40$, C_D is not strongly dependent on stem density and is $O(1)$ [12, 13, 14, 15]. Furthermore, it has been shown that to first order the shape dependence of C_D is negligible and the flow through an array depends primarily on the frontal area a rather than the specific shape of the elements [7, 12]. Because the right-hand side of Eq. 2 is not a function of height above the bed, $C_D a \langle u \rangle^2$ must also be constant over depth. It therefore follows that the velocity varies inversely with the local canopy morphology, represented by $C_D a$:

$$\langle u \rangle(z) = \sqrt{\frac{2g\,\partial\eta/\partial z}{C_D(z)a(z)}} \tag{3}$$

This equation has been shown to correctly predict the velocity profile structure over a salt marsh platform [6]. Note that, because C_D may vary with velocity, the solution to Eq. 3 will require iteration unless a constant C_D can be assumed throughout the canopy.

Eq. 3 implies that when the canopy morphology is heterogeneous, e.g. $C_D a = f(z)$, then the mean velocity $\langle u \rangle = f(z)$ over the same length scale, introducing the possibility of mean-shear dispersion K_a; the subscript a is used to denote the dispersion associated with variation in a. For tracer mixed over depth, i.e. between $z_1 = 0$ and $z_2 = h$, K_a is given by the triple integral relation (e.g., [16]):

$$K_a = -\frac{U}{d(z_2 - z_1)} \int_{z_1}^{z_2} \left(\frac{\langle u \rangle}{U} - 1 \right) \int_{z_1}^{z} \frac{\langle u \rangle d}{D_z} \frac{U}{\langle u \rangle} \int_{z_1}^{z} \left(\frac{\langle u \rangle}{U} - 1 \right) dz\, dz\, dz \tag{4}$$

where D_z is normalized by $\langle u \rangle d$ and $\langle u \rangle$ is normalized by U. Eq. 4 can be predicted from *a priori* knowledge of the canopy morphology as follows. First, the ratio $D_z/\langle u \rangle d$ is a function of $C_D ad$.

If $Re_d > 100$, the wakes of the canopy elements generate turbulence at the scale of the stem, which dominates turbulent diffusion, and the vertical turbulent diffusion is given by [14]:

$$D_z = 0.2\langle u\rangle d\sqrt[3]{C_D a d} \tag{5}$$

where the scale coefficient 0.2 is inferred from data provided by Nepf *et al.* [17]. Further, it follows from Eq. 3 that the velocity ratio $\langle u\rangle/U$ can be expressed in terms of $C_D a$. Using these relations, we can describe the mean-shear dispersion coefficient, K_a, in terms of morphology only:

$$K_a = -\frac{5U}{d(z_2 - z_1)} \int_{z_1}^{z_2} \left(\sqrt{\frac{\overline{C_D a}}{C_d a}} - 1 \right) \int_{z_1}^{z} \left[(C_D a d)^{-1/3} \sqrt{\frac{C_D a}{\overline{C_D a}}} \right] \int_{z_1}^{z} \left(\sqrt{\frac{\overline{C_D a}}{C_d a}} - 1 \right) dz\, dz\, dz \tag{6}$$

The overbar on $\overline{C_D a}$ indicates the value of $C_D a$ corresponding to the depth-averaged velocity U, specifically $\overline{C_D a} = \left[\frac{1}{h}\int_{z_1}^{z_2} (C_D a)^{-1/2}\, dz\right]^{-2}$. Under the action of dispersion, the longitudinal spatial variance of the cloud, σ_x^2, will increase at the rate $d\sigma_x^2/dt = 2K_a$, where K_a is given by Eq. 4 or 6.

Eqs. 4 and 6 can be extended to predict the behavior of tracer in the near field. Before a tracer released at height z_r has mixed over depth, we define its effective vertical scale, Δh, as the equivalent water depth that would yield the same dispersion coefficient at a given longitudinal position, and we let U denote the cross-sectionally averaged velocity over Δh. Based on diffusion scaling, if D_z is constant the effective vertical length-scale of the cloud is expected to increase as:

$$\Delta h = \beta\sqrt{D_z t} \tag{7}$$

where β is an $O(1)$ scale constant. Eq. 7 can be used to define the integration limits for Eqs. 4 and 6. Specifically, at any point in time, the growth rate due to mean-shear dispersion $d\sigma_x^2/dt = 2K_a(t)$ can be calculated by applying Eq. 4 or 6 between $z_1 = z_r - \frac{1}{2}\Delta h$ and

$z_2 = z_r + \frac{1}{2}\Delta h$. Then the evolution of the cloud can be evaluated by alternately applying Eq. 6 (or Eq. 4) and Eq. 7 to predict $\sigma_x^2(t)$.

The appropriate value for the diffusion scale constant β can be determined as follows. Mauri and Haber [18] provide an analytic solution for tracer growth due to dispersion in linear shear, i.e. constant $\partial\langle u\rangle/\partial z$:

$$\sigma_x^2 = \frac{2}{3}\, D_z \left(\frac{\partial\langle u\rangle}{\partial\, z}\right)^2 t^3 \tag{8}$$

where the vertical diffusion is assumed constant over the vertical region of the tracer, which is reasonable for a small cloud. This analytic solution for $\sigma_x^2(t)$ provides an exact point of comparison for $\sigma_x^2(t)$ predicted using numerical integration of Eq. 4. Using a representative field value of $D_z/Ud = 0.2$ [6], the value $\beta = 3.2$ provides the best agreement between the numerical and analytic solutions. This value will be used in all subsequent analysis.

To illustrate the prediction of dispersion from canopy morphology, we consider a simple canopy in which the frontal area per unit volume has a step-function profile, which produces a step-function velocity profile (Fig. 1a). Let a_i, C_{Di}, D_{zi}, and $\langle u\rangle_i$ represent the frontal area, drag coefficient, diffusivity, and horizontally averaged velocity, respectively, in the lower ($i = 1$) and upper ($i = 2$) layers of the canopy. A tracer is released at the interface between the two layers. If $D_{z1} \neq D_{z2}$, the cloud will not grow symmetrically about the interface. We let the vertical scale of the tracer cloud Δh = Δh_1 +Δh_2, where Δh_1 and Δh_2 are the effective vertical extents of the tracer in the lower and upper regions of the canopy, respectively. Applying Eq. 4 between $z_1 = z_r - \Delta h_1$ and $z_2 = z_r + \Delta h_2$, the mean-shear dispersion resulting from the step gradient is:

$$K_a = \frac{\langle u\rangle_1 - \langle u\rangle_2}{8\Delta h}\left(-\frac{(\Delta h_1)^3}{3D_{z1}} + \frac{(\Delta h_1)^2\Delta h_2}{D_{z1}} + \frac{\Delta h_1(\Delta h_2)^2}{D_{z2}} - \frac{(\Delta h_2)^3}{3D_{z2}}\right) \tag{9}$$

Note that we have assumed that $D_z \neq f(z)$ within each layer. In a step canopy with constant stem diameter over depth, $C_D ad$ is constant in each half of the canopy, implying constant D_z

within each layer (Eq. 5). Indeed, a key aspect of turbulence in emergent canopies is that its structure is set by the stem-scale canopy geometry, because the larger structures are damped by the mean canopy drag [6, 14]. In the step profile considered here, despite the strong shear layer formed between the two layers, coherent shear-layer structures were not observed to form [10]. Moreover, White and Nepf [20] confirm that the drag conditions in this canopy are expected to be stable and not produce vortices. In very sparse canopies this condition is not always met, because as the mean drag decreases the shear layer will become unstable and vortices can form at the interface. The exact transition value between the stable and unstable regimes can be determined by stability analysis, as outlined by White [19].

If the vertical diffusion is controlled solely by the local array properties, then Eq. 5 is valid throughout the canopy and is not dependent on mean shear, $\langle u\rangle(z)$. Replacing the effective layer depths in Eq. 9 with $\Delta h_i = \frac{1}{2}\,\beta\sqrt{D_{zi}t}$:

$$K_a = \frac{\beta^2}{48}\left(\frac{\langle u\rangle_1 - \langle u\rangle_2}{U}\right)^2 U^2 t \qquad (10)$$

which is valid for $\Delta h < h$. Note that Eq. 10 predicts that near-field mean-shear dispersion is non-Fickian: K_a increases over time as the cloud increases in size. Using Eq. 3, the velocity difference between the two layers is:

$$\frac{\langle u\rangle_1 - \langle u\rangle_2}{U} = 2\left(\frac{\sqrt{C_{D2}a_2/C_{D1}a_1} - 1}{\sqrt{C_{D2}a_2/C_{D1}a_1} + 1}\right) \qquad (11)$$

so that the near-field dispersion can be predicted from canopy morphology.

When both wake-shear and mean-shear processes are present, their dispersion coefficients add. From Eqs. 1, 10, and 11, the total near-field longitudinal dispersion within the canopy K_x will be given by:

$$K_x = K_d + K_a = \frac{1}{2}Ud\,C_D^{1.5} + \frac{\beta^2}{24}\left(\frac{\sqrt{C_{D2}a_2/C_{D1}a_1} - 1}{\sqrt{C_{D2}a_2/C_{D1}a_1} + 1}\right)^2 U^2 t \qquad (12)$$

Strictly speaking, K_d will differ in the upper and lower regions of the flow, but, anticipating that K_d is only important when the cloud is small and confined to one region of the flow, we make the approximation that $\langle u \rangle \approx U$ and $C_D = f(U)$ for this term. The spatial variance in tracer concentration should therefore evolve such that:

$$\sigma_x^2 = d\, C_D^{1.5}\, x + \frac{\beta^2}{24} \left(\frac{\sqrt{C_{D2} a_2 / C_{D1} a_1} - 1}{\sqrt{C_{D2} a_2 / C_{D1} a_1} + 1} \right)^2 x^2 \tag{13}$$

where we have replaced $x = Ut$. As expected, a canopy in which $C_D a$ has greater variation over depth will produce greater spreading in a tracer cloud. Also note that Eq. 13 shows that the variance grows non-linearly with distance from source. Further, this growth is only weakly dependent, through C_D, on the velocity. If we use the approximation stated earlier that $C_D \approx 1$, the variance can more simply be expressed as:

$$\sigma_x^2 = x\, d + \frac{\beta^2}{24} \left(\frac{\sqrt{a_2/a_1} - 1}{\sqrt{a_2/a_1} + 1} \right)^2 x^2 \tag{14}$$

The variance will continue to increase non-linearly until $\Delta h_1 = \Delta h_2 = h/2$, after which K_a will reach a constant value given by Eq. 6 with $z_1 = 0$ and $z_2 = h$, and the spatial variance will continue to increase linearly in space and time.

Methods

Velocity measurements and dye studies were conducted in a 6.7-m-long, 20.3-cm-wide, 30.5-cm-tall rectangular plexiglass flume. Over multiple runs, the water depth $h = 20 \pm 1$ cm. Wooden circular dowels with a diameter $d = 0.64$ cm were arranged randomly in a 6.1-m-long perforated plastic sheet and suspended from the top of the flume toward the bed. Half of the dowels extended only to mid-depth, creating a canopy with two layers, $n_1 = 300$ m^{-2} and $a_1 d = 0.012$ in the lower layer and $n_2 = 600$ m^{-2} and $a_2 d = 0.024$ in the upper layer.

Depth-averaged flow speeds ranged from 0.75 to 4.3 cm s^{-1}.

Due to instrument availability, velocity was measured using both laser Doppler velocimetry (Dantec, Mahwah, New Jersey) and acoustic Doppler velocimetry (SonTek/YSI, Inc., San Diego, California). A five-minute velocity record was taken at each of 11–14 vertical positions at least 2.8 m downstream of the start of the array. A 5-cm-wide swath of dowels was cleared to prevent interference with the laser beams or probe head. This length scale is comparable to the mean stem spacing, so it has a negligible effect on the local mean flow [21]. To sample horizontal heterogeneity, vertical velocity profiles were repeated at six different horizontal locations within the array. The measured velocity and resulting turbulence statistics at each depth were then averaged to remove the stem-scale spatial heterogeneity. Smoothed spectra were calculated using a Parzen window.

Longitudinal dispersion was explored using slug releases of dye at mid-depth ($z_r = 10$ cm). Rhodamine WT or Rhodamine 6G was released from tygon tubing oriented parallel to the direction of flow. Releases took 0.5–2 s each, which was much less than the travel time to the fluorometer (22–745 s), so the releases were assumed to be instantaneous. The release velocity was matched to the ambient velocity with the help of a syringe pump. The recording fluorometer was positioned at mid-width, mid-depth, and 50 to 525 cm downstream of the release point. Between 5 and 29 slug releases were performed at between 5 and 8 travel distances at each of four flow rates, and the results were averaged to describe the ensemble mean behavior for each flow rate. Temporal variance was calculated for each concentration record after normalization by the total area under the curve, which makes the shape of the profile independent of the initial mass, lateral and vertical diffusion, and the lateral position of the cloud center [10].

Results

For all flow rates, water moved faster in the lower, sparser canopy (z = 0–10 cm, $a_1 d = 0.012$) than in the upper, denser canopy (z = 10–20 cm, $a_2 d = 0.024$; see Table 1). As Fig. 2 shows for the slowest and fastest flow conditions, the bottom boundary layer was confined to within 1 cm of the bed. The horizontally averaged velocity, $\langle u \rangle$, was approximately constant over depth within each layer of the canopy, and the narrow interfacial region had a width (≈ 2 cm) that was approximately constant over distance, x (Fig. 2). Many of the velocity spectra (not shown) contained a shoulder near 1 Hz, corresponding to the frequency of vortex shedding. However, no larger, coherent structures were indicated by the spectra, confirming that the array drag damped turbulence at scales greater than the stem diameter, d. This confirms the assumption in Eq. 5 that transport is dominated by stem-scale turbulence.

Table 1 presents the velocity ratio $\left(\langle u \rangle_1 - \langle u \rangle_2\right)/U$ along with the velocity ratio predicted from the distribution of $C_D a$ using Eq. 11 and estimating C_D with an isolated cylinder formula ($C_D = 1 + 10 Re_d^{-0.66}$ [11]). For the highest flow condition, the observed and predicted values match, confirming that for $Re_d > 100$ and $ad < 0.1$ the isolated cylinder equation successfully predicts the drag in an array. For the lowest flow condition, the mean predicted ratio is only half of the observed ratio (Table 1). This difference reflects the departure of C_D from the values obtained from the isolated cylinder equation for the low Re_d regime in the upper layer of the canopy ($Re_{d2} = 25 \pm 4$). Koch and Ladd [13] have shown that, for $Re_d < 40$, the value of C_D in a random array of cylinders is as much as five times the value predicted using a single-cylinder approximation. Although insufficient data are available to confidently adjust C_D for different combinations of Re_d and ad, the observed velocity ratio would be predicted if C_D in the upper canopy were triple that calculated using a single-cylinder equation, which seems quite plausible given the results from Koch and Ladd [13].

Fig. 3 shows measurements of spatial variance as a function of distance from release. Spatial variance increases non-linearly with distance at all flow rates, confirming that the dominant dispersive processes have not reached their Fickian limit. The dotted line in Fig. 3 represents the predicted increases in spatial variance due to stem-shear dispersion (Eq. 1). For this canopy it is expected that the stem-scale dispersion reaches its Fickian limit after a distance of $x \approx a^{-1} \approx 8$ cm. The tracer variance predicted in a step profile from the sum of stem-scale and mean-shear processes (Eq. 13 with $\beta = 3.2$) is included in Fig. 3 as a solid line. This curve, which is not calibrated, shows very good agreement with the observations, supporting the above theory. Even so, note that the prediction tends to underestimate σ_x^2 for the lowest velocity case, consistent with the observation that the isolated cylinder approximation for the drag coefficient underestimates $\left(\langle u \rangle_1 - \langle u \rangle_2\right)/U$ for this flow condition. The dashed lines shows that assuming $C_D = 1$ throughout the canopy (Eq. 14) also provides a reasonable prediction, suggesting that this method is relatively robust toward the exact value of C_D in an array. Note that mean-shear dispersion is predicted to become larger than stem-shear dispersion approximately 100 cm downstream of the release; beyond this location mean-shear dispersion dominates.

Discussion

Within an emergent canopy of sufficient canopy density, vegetative drag controls the flow structure, so that the morphology, specifically $C_D a(z)$, can be used to predict the longitudinal velocity $\langle u \rangle(z)$ (Eq. 3). Because the vertical turbulence and thus diffusion are also principally a function of the local canopy morphology (Eq. 5), the dispersive spread of a tracer cloud in the near field can be predicted from canopy morphology alone (Eq. 6). The measurements shown here confirm this approach for a step profile in $C_Da(z)$. A step profile is a simple geometry with a readily derivable analytic solution, and it also represents the maximum shear in a canopy with a known range of C_Da. Values of C_Da were chosen to mimic values found in real wetlands. Other recent work has confirmed this approach in the field in a canopy of the salt grass *Spartina alterniflora* [6].

We now consider differences in the growth of tracer variance in three representative canopies with different $C_Da(z)$. For comparison, the average velocity U and the difference between the maximum and minimum velocities $\Delta\langle u\rangle$ are the same in all three canopies (Fig. 1). A step $\langle u\rangle(z)$ profile (Fig. 1a) approximates flow in a mangrove canopy [12]; K_a in this canopy is calculated using Eq. 10. The mid-depth regions of a *S. alterniflora* canopy exhibit $a \sim z^{-1/2}$, which produces a locally linear velocity profile [6, 22] as shown in Fig. 1b; variance growth due to mean-shear dispersion in this canopy follows Eq. 8. The velocity profile shown in Fig. 1c was rescaled from that measured by Vermaat *et al.* [23] in an *Alisma gramineum* canopy. For this canopy the growth in spatial variance due to mean-shear dispersion can be calculated by numerical integration of Eq. 4, with the vertical width of the cloud at each time step determined using Eq. 7 with $\beta = 3.2$. For all three canopies, the total expected growth in spatial variance will result from the sum of stem-scale and mean-shear dispersion; variance growth due to stem-scale dispersion follows $d\sigma_x^2/dt = 2K_d$, where K_d is given by Eq. 1.

Fig. 4 shows the evolution of an instantaneous point release at mid-depth for all three canopies including both stem-scale and mean-shear processes and assuming typical field values of $D_z/Ud = 0.2$ and $U = 1$ cm s^{-1} [6]. After the center of mass of the cloud has traveled 10 m downstream, its vertical dimension will be approximately 11 cm (Eq. 7). At this point, the longitudinal extent of the cloud, $4\sigma_x$, is predicted to be 11 m in a canopy with a step velocity profile, 5 m in an *A.gramineum* canopy, and only 3 m in a canopy with a linear velocity profile.

This difference in cloud sizes can have important implications for transport in the near field. For example, many larvae are passively transported by water currents [24], and increased dispersion will result in an increased spread of propagules. In addition, many crustacean species depend on tracing odor plumes to find food sources, and reduced dispersion will result in the increased persistence of an odor plume [25].

The differences in vertical velocity profiles created by different vegetation canopies thus have an important impact on the spread of transported constituents in the near field. Eq. 6 provides a way to estimate this growth for any canopy morphology. Note that, because a step velocity profile produces the maximum dispersion, Eq. 13 estimates the maximum potential of growth given only the minimum and maximum $C_D a$ values in the canopy. Similarly, the linear prediction can provide a reasonable lower bound. Finally, the method is reasonably successful even when only the frontal area distribution $a(z)$ is known (i.e., Eq. 14).

Acknowledgements

The authors are grateful to Amanda Sorenson and Alessandro Papa for their assistance in data collection and to two anonymous reviewers for their comments. A. F. L. was supported by a National Defense Science and Engineering Graduate Fellowship and a National Science Foundation Graduate Research Fellowship. The equipment and H. M. N. were supported by the National Science Foundation under Grant EAR 0309188. Any opinions, findings, or recommendations expressed in this material are those of the authors and do not necessarily reflect the views of the National Science Foundation.

References

[1] Stage, S.A.: 2004, Determination of acute exposure guideline levels in a dispersion model, *J. Air Waste Manage. Assoc.* **54**, 49–59.

[2] Fonseca, D.M. and Hart, D.D.: 1996, Density-dependent dispersal of black fly neonates is mediated by flow, *Oikos* **75**, 49–58.

[3] Middleton, B.: 2000, Hydrochory, seed banks, and regeneration dynamics along the landscape boundaries of a forested wetland, *Plant Ecol.* **146**, 169–184.

[4] Finelli, C.M.: 2000, Velocity and concentration distributions in turbulent odor plumes in the presence of vegetation mimics: a flume study, *Mar. Ecol. Prog. Ser.* **207**, 297–309.

[5] Leonard, L.A. and Luther, M.E.: 1995, Flow hydrodynamics in tidal marsh canopies, *Limnol. Oceanogr.* **40**, 1474–1484.

[6] Lightbody, A.F. and Nepf, H.M.: 2006, Prediction of velocity profiles and longitudinal dispersion in emergent salt marsh vegetation, *Limnol. Oceanogr.* **51**, 218–228.

[7] Mazda, Y., Wolanski, E., King, B., Sase, A., Ohtsuka, D. and Magi, M.: 1997, Drag force due to vegetation in mangrove swamps, *Mangroves and Salt Marshes* **1**, 193–199.

[8] Ayotte, K.W., Finnigan, J.F. and Raupach, M.R.: 1999, A second-order closure for neutrally stratified vegetative canopy flows, *Boundary-Layer Meteorol.* **90**, 189–216.

[9] White, B.L. and Nepf, H.M.: 2003, Scalar transport in random cylinder arrays at moderate Reynolds number, *J. Fluid Mech.* **487**, 43–79.

[10] Lightbody, A.F.: 2004, *Field and laboratory observations of small-scale dispersion in wetlands*, MS thesis, Mass. Inst. of Tech., Cambridge, Massachusetts.

[11] White, F.M.: 1991, *Viscous Fluid Flow*, McGraw-Hill, New York.

[12] Struve, J., Falconer, R.A. and Wu, Y.: 2003, Influence of model mangrove trees on the hydrodynamics in a flume, *Estuar. Coast. Shelf Sci.* **58**, 163–171.

[13] Koch, D.L. and Ladd, A.J.C.: 1997, Moderate Reynolds number flows through periodic and random arrays of aligned cylinders, *J. Fluid Mech.* **349**, 31–66.

[14] Nepf, H.M.: 1999, Drag, turbulence, and diffusion in flow through emergent vegetation, *Water Resour. Res.* **35**, 479–489.

[15] Stone, B.M. and Shen, H.T.: 2002, Hydraulic resistance of flow in channels with cylindrical roughness, *J. Hydraul. Eng.* **128**, 500–506.

[16] Fischer, H.B., List, E.J., Koh, R.C.Y., Imberger, J. and Brooks, N.H.: 1979, *Mixing in Inland and Coastal Waters*, Academic Press, San Diego.

[17] Nepf, H.M., Sullivan, J.A. and Zavistoski, R.A.: 1997, A model for diffusion within emergent vegetation, *Limnol. Oceanogr.* **42**, 1735–1745.

[18] Mauri, R. and Haber, S.: 1986, Applications of Wiener’s path integral for the diffusion of Brownian particles in shear flows, *SIAM J. Appl. Math.* **46**, 49–55.

[19] White, B.L.: 2006, Momentum and mass transport by coherent structures in a shallow vegetated shear flow, Ph.D. thesis, MIT, Cambridge, Massachusetts.

[20] White, B. L. and Nepf, H. M.: 2006, Shear instability and coherent structures in shallow flow adjacent to a porous layer, *J. Fluid Mech.*, submitted.

[21] Ikeda, S. and Kanazawa, M.: 1996, Three-dimensional organized vortices above flexible water plants, *J. Hydraul. Eng.* **122**, 634–640.

[22] Neumeier, U. and Ciavola, P.: 2004, Flow resistance and associated sedimentary processes in a *Spartina maritima* salt-marsh, *J. Coast. Res.* **20**, 435–447.

[23] Vermaat, J.E., Santamaria, L. and Roos, P.J.: 2000, Water flow across and sediment trapping in submerged macrophyte beds of contrasting growth form, *Arch. Hydrobiol.* **148**, 549–562.

[24] Harii, S., and Kayanne, H.: 2003, Larval dispersal, recruitment, and adult distribution of the brooding stony octocoral *Heliopora coerulea* on Ishigaki Island, southwest Japam, *Coral Reefs* **22**, 188–196.

[25] Moore, P., and Crimaldi, J.: 2004, Odor landscapes and animal behavior: tracking odor plumes in different physical worlds, *J. Mar. Sys.* **49**, 55–64.

Figure 1 Sample distributions of $C_D a(z)$ and the corresponding horizontally and temporally averaged velocity $\langle u \rangle(z)$ for three emergent canopies, with gray tracer clouds in the near field: (a) the step frontal area distribution considered in this paper is a good representation of an inverted mangrove forest [7, 12]; (b) a region of the frontal area profile for a *Spartina alterniflora* canopy with the volumetric frontal area density $a \sim z^{-1/2}$, which produces a linear velocity profile [6]; and (c) velocity measurements (points), fitted velocity curve, and inferred frontal area density (Eq. 3) in a canopy of *Alisma gramineum* (velocity data from Vermaat *et al.* [23]).

Figure 2 Vertical profiles of longitudinal velocity for (a) the slowest flow condition and (b) the fastest flow condition. Horizontal bars indicate the standard error of the mean across the canopy heterogeneity. The point with no bars is the time-averaged velocity at a single location; its error is expected to be comparable to that of the points directly below it.

Figure 3 The spatial variance of dye clouds released at the interface as a function of distance from release for different flow conditions: mean dye velocity at the interface of (a) 0.8 ± 0.1 cm s^{-1}, (b) 2.0 ± 0.1 cm s^{-1}, (c) 3.1 ± 0.1 cm s^{-1}, and (d) 4.1 ± 0.1 cm s^{-1}. The curves indicate predictions based on canopy morphology: the dotted lines are predicted using the stem-shear dispersion coefficient K_d (Eq. 1), the solid lines are predicted from the sum of the stem-shear and mean-shear dispersion coefficients, $K_d + K_a$, including a depth-varying drag coefficient, $C_D = f(z)$ (Eq. 13), and the dashed lines are predicted from $K_d + K_a$ assuming $C_D = 1$ (Eq. 14).

Figure 4 The evolution of tracer variance predicted for a slug released into a flow with a depth-averaged velocity $U = 1$ cm s^{-1} and the three velocity profiles shown in Figure 1: step velocity profile with dispersion predicted using Eq. 10, velocity profile within a canopy of *Alisma* *gramineum* with dispersion predicted using Eq. 4 (velocity data from Vermaat *et al.* [23]), and linear velocity profile with cloud growth predicted using Eq. 8.

Table 1: Average velocity and drag characteristics (mean $\pm$ standard error of the mean) in each layer for the slowest and fastest flow conditions. Drag coefficients are calculated using a single-cylinder equation [11] and include 20% error to account for spatial variability within the canopy.

Flow variable	Location	Flow condition	
		Slowest	Fastest
Velocity (cm s^{-1})	Lower canopy, $\langle u \rangle_1$	1.1 ± 0.1	5.2 ± 0.1
	Upper canopy, $\langle u \rangle_2$	0.4 ± 0.1	3.4 ± 0.1
	Depth average, U	0.8 ± 0.1	4.3 ± 0.2
Reynolds number	Lower canopy, Re_{d1}	73 ± 2	332 ± 8
	Upper canopy, Re_{d2}	25 ± 4	221 ± 8
Drag coefficient	Lower canopy, C_{D1}	1.6 ± 0.3	1.2 ± 0.2
	Upper canopy, C_{D2}	2.2 ± 0.5	1.3 ± 0.3
$(\langle u \rangle_1 - \langle u \rangle_2)/U$		1.0 ± 0.1	0.4 ± 0.1
$2\left(\frac{\sqrt{C_{D2}a_2/C_{D1}a_1}-1}{\sqrt{C_{D2}a_2/C_{D1}a_1}+1}\right)$		0.5 ± 0.1	0.4 ± 0.1

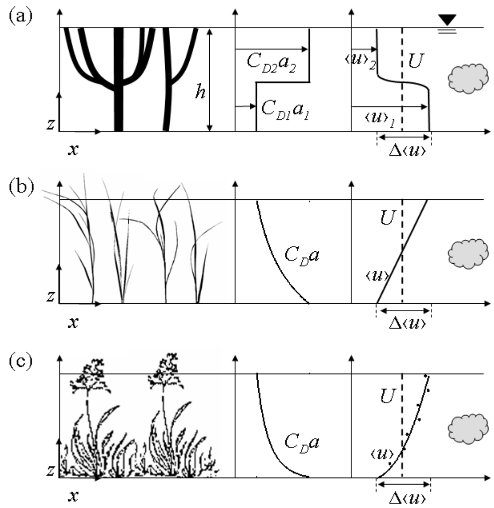

Figure 1: Lightbody and Nepf

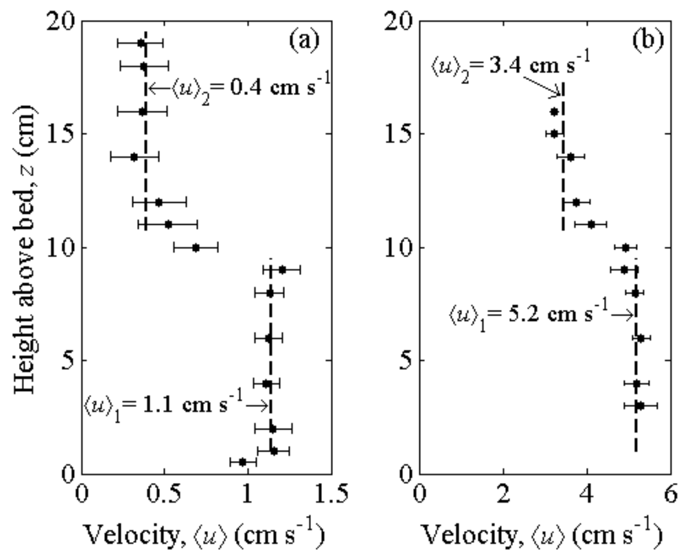

Figure 2: Lightbody and Nepf

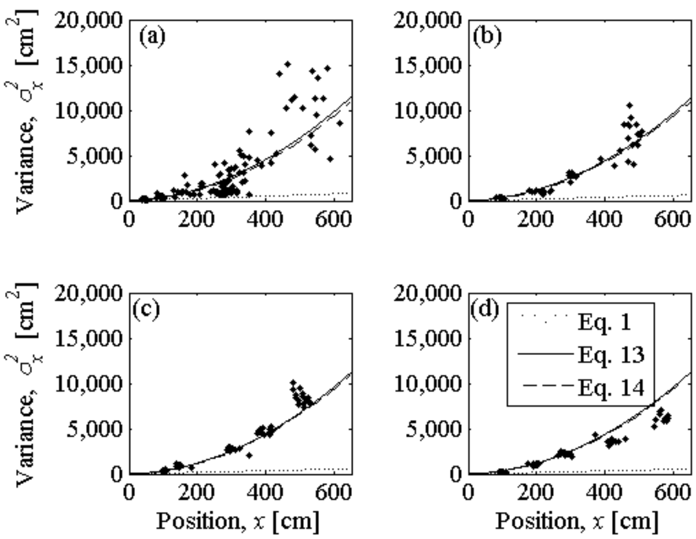

Figure 3: Lightbody and Nepf

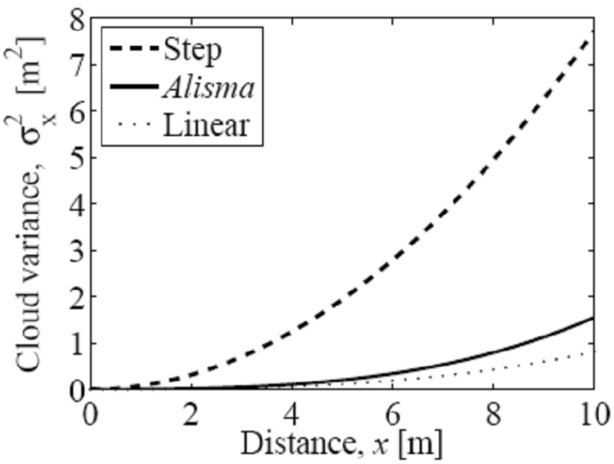

Figure 4: Lightbody and Nepf